New Hull-Voxel Approach to Image Reconstruction from Limited Projections and Views

Valeriy VENGRINOVICH , Sergei ZOLOTAREV, Institute of Applied Physics, Minsk, Belarus
Wolfgang SCHLEGEL, Bernd-Michael HESSE, German Center for Cancer Research(DKFZ), Heidelberg, Germany
Juergen HESSER, Mannheim University, Mannheim, Germany

Abstract. We discuss the problem of image reconstruction from limited views and sparse projections in order to achieve a more accurate diagnosis of the patient's morphology. As a priori assumption we demand that the object consists of regions with constant attenuation coefficient. Hereby, the number of such regions is not restricted. The dual-phase reconstruction concept is a new method based on this a priori information and thus allows counterbalancing for to the lack of projections data. In the first reconstruction phase the Bayesian approach is applied while at the second phase the so called hull-voxel iteration technique is developed which provides the iterative fitting of region surfaces by global optimization. The results are evaluated based on simulated Shepp-Logan and experimental medical phantoms respectively.

Introduction

Image reconstruction from incomplete and noisy X-Ray projections yields increasing attention, intensified by clear practical demands for reduced radiation dose; real time tracking of e.g. a tumor, organ or a technical party. This trend towards the development of image reconstruction algorithms and tools which would operate with incomplete data sets is as well encouraged by the transition from fan to cone beam data acquisition and local tomography cases.

If the ROI is easily seen from sufficient set of x-ray projections, then one of the available techniques, either based on the classical Radon transformation, see for fundamentals e.g. [1], or iterative approaches, see for the tutorial [2], can be used for reconstruction. However, in a case of limited angles or limited number of projections, or both, the problem becomes extremely ill-posed. Traditional algorithms are unable to achieve an artifact-free reconstruction and often lead to severe image blurring in the direction of X-ray propagation whereby the blurring increases with fewer projections and smaller viewing angles.

The limited angle problem is much more critical than sparse projections. The Bayesian technique, complemented by efficient prior knowledge, is recognized as one of the most powerful tools for image reconstruction from limited data sets [3]. Statistical properties as

prior for Bayesian reconstruction, being very productive for binary images [4-6], are less efficient in compensating for missed data, especially in case of low contrast medical images.
We consider the case of a portal-type data acquisition Setup with the position of kV source at the opposite side of an object with regard to MEV accelerator target [8] (Fig.1). The acquisition geometry (Fig.2) is provided by a circular (around vertical axes) or line (along a horizontal line) trajectory of a x-ray source. In case of a circular trajectory the admissible solid angle for object observation cannot exceed 90^0 and thus one have to deal with a limited angle problem.
In this article we present a dual-phase constrained 3D image reconstruction technique of a region of interest (ROI), which can overcome an image degradation resulting from limited data. This technique is named Dual-phase Shell-Voxel Iterative Reconstruction (SVIR) from limited views and sparse projections. The existence of sharp 3D shells, which cover voxels with uniform attenuation coefficients respectively, is incorporated by the SVIR algorithm as the basic prior information.

SVIR algorithm

The idea is based on some prior assumptions:

- 3D image of an object is given by a limited number of 2D x-ray projections. Example is shown in fig.1 and 2 where the imager is non movable while the x-ray source is moving in a parallel (to the imager) plane within a solid angle α.

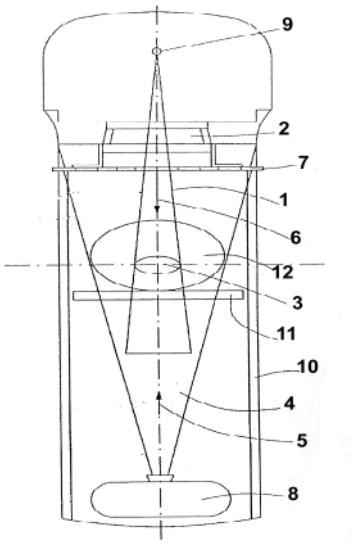

Fig.1.Chart of the combined Radiation Therapy&Diadnostic Setup: 1-therapy beam; 2-Multi Leaf Collimator; 3-ROI with tumor; 4-kV beam; 5- main Setup axle; 6-therapy beam direction; 7-2D imager; 8-kV X-ray tube; 9-MEV photon target; 10-gantry; 11-couch; 12-patient.

- an object consisting of constituents (regions) is assumed, each constituent being defined by a closed surface - hull;
- within each constituent, called “Constituent Domain” (CD), the x-ray attenuation coefficient is uniform;
- the number of given CDs and their respective attenuation coefficients are not restricted;
- an operator may extract a ROI which is of main interest on one's own.

The SVIR algorithm consists of a dual-phase procedure having in the first phase the mechanism of iterative Bayesian image reconstruction considering 3D image as a lattice system [2]. At the second phase the fitting of constituents’ surfaces (hulls) is applied to a selected ROI iteratively, subject to the constraint of uniform ACs within CD of an interest.
For digitization purposes the reconstructed object is split-up into voxels whose positions are defined in the Cartesian coordinate system. A connected group of voxels with uniform attenuation coefficient forms a CD, that is covered by a hull. The shapes of CDs and their attenuation coefficients are unknown and are flexible during each iteration step. CDs, like e.g. tumor, subjected to accurate reconstruction, are specified by an operator or automatically

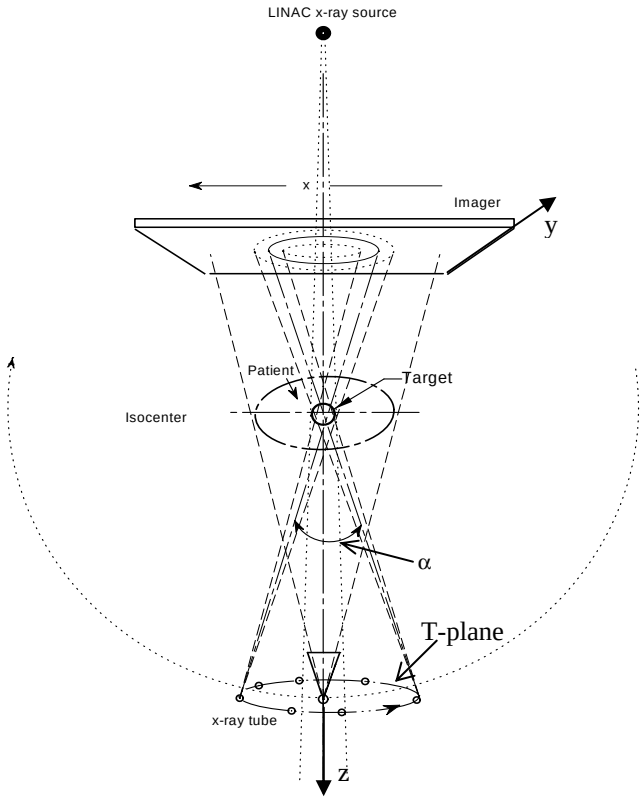

Fig. 2. Data acquisition geometry outline. Trajectory of an X-ray tube is parallel to the detector plane, α - solid angle.

before starting second phase.

For the x-ray linear attenuation model the ray sum $p_{n,i}$ in the i-th pixel of the 2D detector is calculated as a linear integral of unknown absorption coefficients along this ray. The discrete form of this model is as follows:

$$p_{n,i} = \sum_{j=1}^{J} \mu_j l_{n,ij}; n = \overline{1,N}; i = \overline{1,I}; j = \overline{1,J} \quad (1)$$

where N is the number of projections, I is the number of detector pixels, J is the number of voxels in a ROI under reconstruction; μ_j - is the underlying set of unknown attenuation coefficients in corresponding voxels j.

1st step: Bayesian image reconstruction

The operator form of the discrete equation (1) is given by:

$$p(y) = O\mu(x), \quad (2)$$

where O – operator describing the x-ray propagation model.

In case of limited data equation (2) is always ill-posed. It is solved by the iteration equation

$$\hat{\mu} = \arg\min_{\mu} \left\{ \left\| O\tilde{\mu}(x) - p(y) \right\|^2 + \alpha B(\tilde{\mu}) : \mu(x) \in R^n \right\} \quad (3)$$

where R^n – n-dimensional Euclidian space, $O\tilde{\mu}(x)$ - simulated or mock data. $B(\tilde{\mu}) = -\ln P(\tilde{\mu})$ - prior description and prediction of a tested object. $B(\mu)$ is a quality constraint (prior knowledge) imposed on the solution. α is the regularization coefficient which varies in the range from 0 to 1

In the literature on statistical image recovery from few radiographs several forms of priors are recommended. Within our approach, the qualitative a priori knowledge is integrated in the form of the mean square difference between the gray levels in each voxel and its neighboring voxels (it may be also considered as Gibbs prior of the first order):

$$B(\mu) = \sum_{j=1}^{J} \sum_{a=1}^{A} \left(\mu_j - \mu_{j,a} \right)^2 \quad (4)$$

where index a defines a voxel adjacent to the j-th one.

The minimization of this functional is implemented by conjugate gradients [2] with an iteration-stopping criterion in the form of assumed minimum discrepancy. As result a rough 3D intermediate image is obtained, containing artifacts and blurred regions as mentioned (see Fig.3b to Fig.5b).

3. 2nd phase: image reconstruction using hull-voxel iteration procedure.

Given a starting image the second phase of the SVIR procedure begins with labeling of an area in each CD of interest by small dot. This dot stands as a nucleus of a corresponding

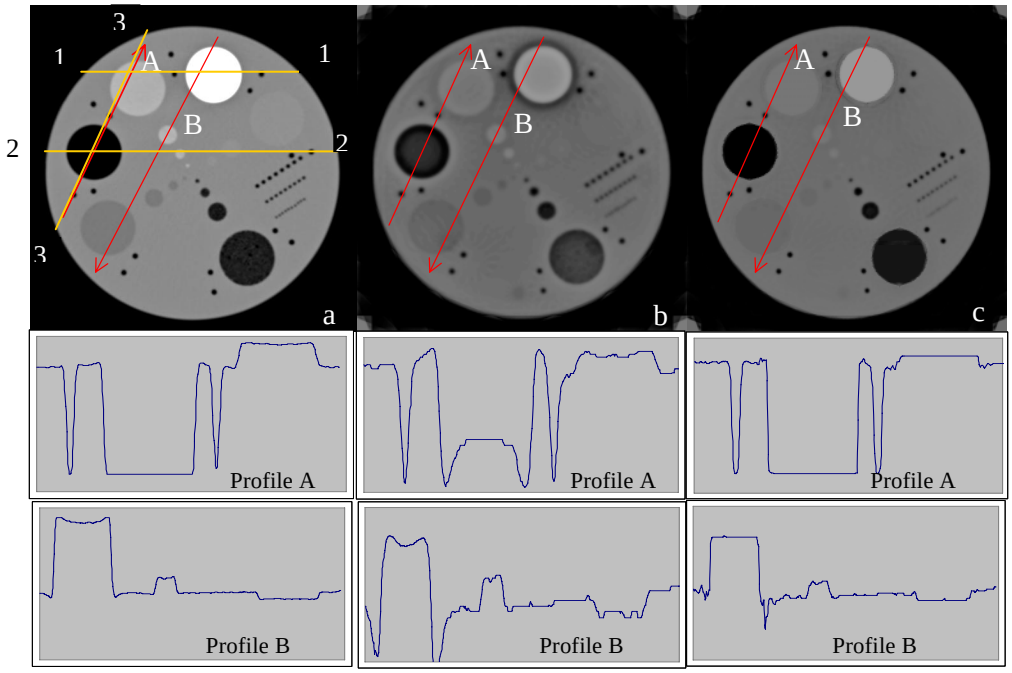

Fig.3. Columns a), b) and c) illustrate the results of application of three image reconstruction techniques, respectively: a) FBP technique from 720 cone-beam x-ray projections, taken within traditional CT acquisition geometry, b) Bayesian technique from 20 cone-beam projections taken within planar acquisition geometry, solid angle $\alpha=90^0$ (Fig.2); c) SVIR within the same acquisition as (b). Upper row: XOY central frontal slice in the 3D image of the kugel-like phantom in Fig.3, reconstructed by three reconstruction techniques a), b) and c) in respective columns. Middle and bottom rows show the gray level profiles along the arrows A and B respectively. The proximity of images and shapes of the profiles in the columns a) and c) illustrate the advantage of the SVIR algorithm comparing to the Bayesian (b).

constituent (e.g. tumor) image during subsequent iteration procedure. The number of labeled CDs is non limited. The labeling can be done either manually in a display or automatically by appropriate segmentation. The boundaries of this sphere form a shell that “propagates” during iterations.

SVIR algorithm validation based on experimental 3D data including noise

For benchmark reasons the Bayesian and second-phase algorithms were tested using x-ray experimental data. The kugel-like phantom was filled with a water-like matrix material and its attenuation coefficient was defined equal 1. Its frontal XOY cross section is seen in Fig.3. Six disks, each 30 mm diameter and 10 mm thickness, were inserted in the matrix at its equator. Six disks’ materials had attenuation coefficient 0.25; 0.75; 0.02; 1.1; 2.3 and 0.9 respectively (calculated clockwise from the separated one). Four self-similar groups of small cylinders inside the disks were machined, three of them, with diameters 10, 5 and 2 mm respectively, and were filled with the same materials as the closest disk. The rest of cylinders were filled with air.
700 cone-beam projections have been captured in an usual CT acquisition geometry, and 3D image of the phantom was reconstructed by traditional Filtered Back Projection (FBP) technique. The restored image of the frontal cross-section in the XOY plane is shown in

Fig.3a. In the Fig.4a to Fig. 5a the images of slices are shown, which are cross-cuts 1-1, 2-2 and 3-3 perpendicular to XOY plane. They give a typical insight of the phantom structure and the attenuation coefficient distribution. The corresponding positions of the slices are noted in the figures captions. The gray value profiles along some selected directions, which are shown in the figures by arrows, are plotted left, right or below each image. Each cone-beam projection had the capacity of 220x280 pixels each of 0.825x0.825 mm size. The reconstructed region occupied the volume of 512x512x30 voxels each of 0.35x0.35x1.0 mm size.

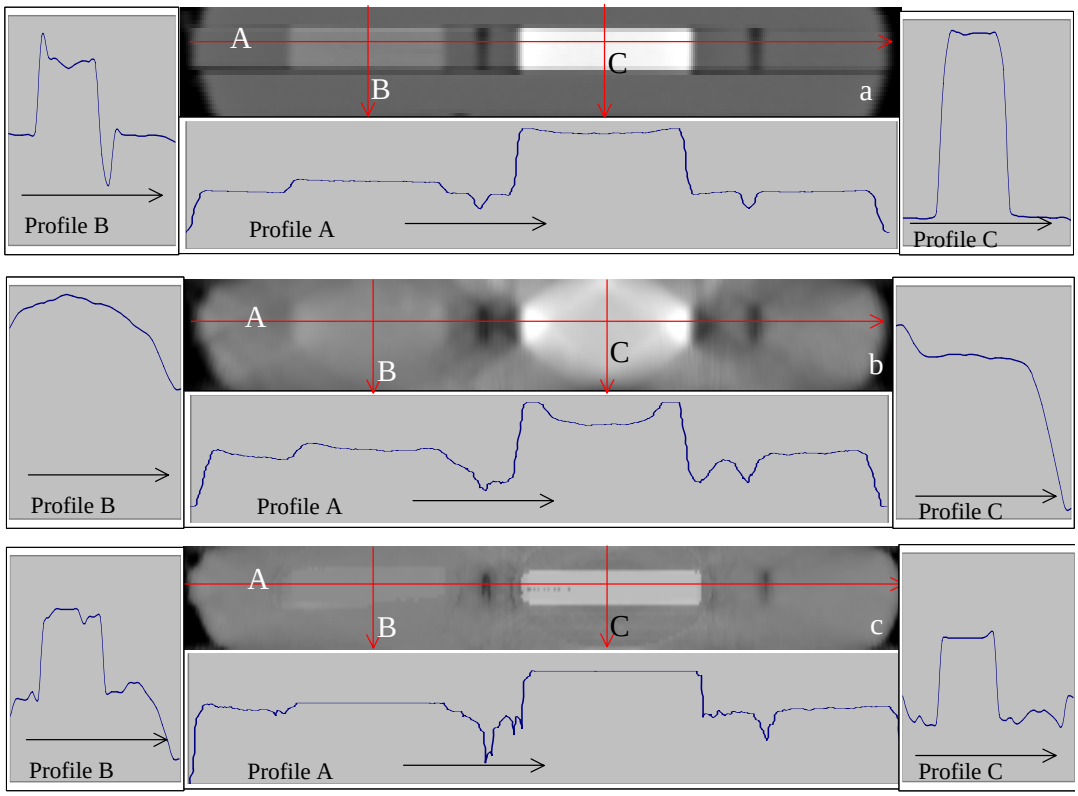

Fig.4. Slice 1-1 in the Fig.5. Rows a), b) and c) illustrate the results of application of three image reconstruction techniques, respectively: a) FBP technique from 720 cone-beam x-ray projections, taken within traditional CT acquisition geometry, b) Bayesian technique from 20 cone-beam projections taken within planar acquisition geometry, solid angle $\alpha=90^0$ (Fig.2); c) SVIR within the same acquisition as (b). A, B and C arrows on the images represent the directions of gray level profiles shown in three columns respectively: central, left and right. The proximity of images and shapes of the profiles in the rows a) and c) illustrate the advantage of the SVIR algorithm comparing to the Bayesian (b). In the row (c) the artifacts and blurring in two labeled disks is avoided unlike in the row (b).

The CT images (Fig. 4a to Fig.5a) were the basis for computing 18 projections uniformly distributed in the T-plane within the planar acquisition geometry shown in the Fig. 2. The forward projections were calculated in correspondence with the eq. (1). The cone solid angle β was 90^0. Finally, those, reduced by factor more than 40 (comparing to CT), noisy data were used for the image reconstruction of the ROI using the Bayesian Image Reconstruction (BIR) technique and the HVR. The results from both methods are shown in the Fig. 4b and 4c to Fig. 5b and 5c respectively. Only three labeled CDs, having the attenuation coefficients 0.02; 1.1 and 2.3, are shown in the figures. The impact of labeling is observed while comparing the

quality of the reconstructed images of labeled disks and non labeled filled and non filled cylinders. (We don't show here the phantom images, restored from limited data by FBP algorithm, since the Bayesian algorithm with a priori knowledge in the form of a Gibbs prior of the first order (Fig. 4b to Fig. 5b) gives much better image quality than FBP).

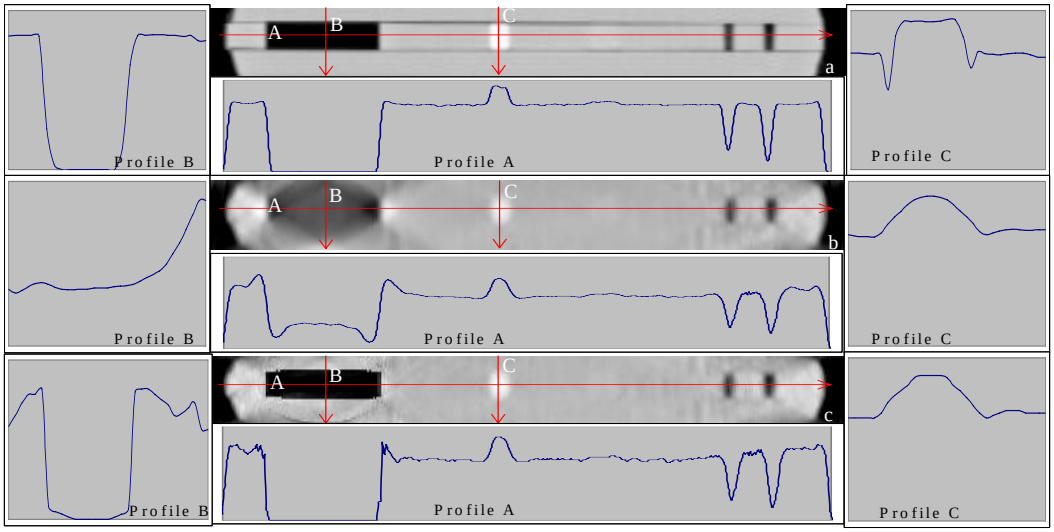

Fig.5. Slice 2-2 in the Fig.5. Rows a), b) and c) illustrate the results of application of three image reconstruction techniques, respectively: a) FBP technique from 720 cone-beam x-ray projections, taken within traditional CT acquisition geometry, b) Bayesian technique from 20 cone-beam projections taken within planar acquisition geometry, solid angle $\alpha=90^0$ (Fig.2); c) SVIR within the same acquisition as (b). A, B and C arrows on the images represent the directions of gray level profiles shown in three columns respectively: central, left and right. The proximity of images and shapes of the profiles in the rows a) and c) illustrate the advantage of the SVIR algorithm comparing to the Bayesian (b). In the row (c) the artifacts and blurring in two labeled disks is avoided unlike in the row (b).

Conclusion

Simple visual analysis of images produced with Bayesian and SVIR algorithms (Fig. 4b and 4c to Fig. 5b and 5c) respectively with the CT images (Fig. 4a to Fig. 5a) show the advantages of SVIR algorithm.:

- The most critical blurring of labeled CDs in Z-axis direction is mostly removed;
- The proximity of the gray value profiles obtained by SVIR to those obtained traditional CT is much better;
- The artifacts caused by the limited observation angle have mostly vanished in the labeled CDs;
- The calculation time is strongly decreased due to the reduction of the dimensionality: the number of iterated vertexes compared to voxels is by orders of magnitude less.

The drawback of the proposed technique results from the assumed constraints i.e. the assumption of domains existence with homogenous attenuation coefficients.
Some aspects of the developed algorithm should be investigated in future, mainly its applicability for different kinds of objects. Other aspects are the robustness against noise and labeling arbitrariness, optimal segmentation procedure for automatic labeling, speedup in reconstruction.

At the end we can draw the conclusion that the new image reconstruction technique for very limited observation angle and sparse projections has many advantages in comparison with the most comprehensive Bayesian as well as Filtered Back Projection techniques.

References

[1] F.Natterer. The Mathematics of Computerized Tomograthy. John Wiley&Sons, Chichester, USA, and B.G.Teubner, Stuttgart, Germany, 1986.

[2] W.H.Press, S.A.Teukolsky, W:T.Wetterling and B.P.Flannary. Numerical Recipes in C. Cambridge, University Press, 1992.

[3] J.Fessler. "Statistical image reconstruction methods for transmission tomography", in "Handbook of medical imaging, Vol.2. Medical image processing and analysis" M.Sonka and J.M.Fitzpatrick, editor. SPIE, Bellingham, pp.1-70, 2000.

[4] K.M.Hanson. Bayesian and related methods in image reconstruction from incomplete data. In *Image recovery: Theory and Applications, H.Stark ed.Academic, Orlando.* 79-125, 1987.

[5] V. Vengrinovich, Yu. Denkevich, and G.-R. Tillack. Reconstruction of Three-Dimensional Binary Structures from an Extremely Limited Number of Cone-Beam x-ray Projections. Choise of Prior. *Journal of Phys., D:Applied Physics*. V.32 pp. 2505-2514, 1999

[6] V. Vengrinovich, Yu. Denkevich, and G.-R. Tillack. Bayesian 3D x-ray reconstruction from incomplete noisy data. In book: *Maximum Entropy and Bayesian Methods*, ed. by W.von der Linden et. al., Kluwer Academic Publishers, pp. 73-83, 1999.

[7] V. Vengrinovich, Yu. Denkevich, G.-R. Tillack, U.Ewert and B.Redmer. Bayesian Restoration of Crack Images in Welds from Incomplete Noisy Data. *Review of Progress in QNDE*, ed. by D. O. Tompson and D. E. Chimenti, v. 19A, American Institute of Physics, Melville-N.Y., pp.635-642, 2000.

[8] Hesse, Bernd-M. "Device for performing and verifying a therapeutic treatment and corresponding computer program and control method" **WO 03/076016 A1, 2003**.